Visual Abstract

Influence of additional static stresses on biaxial low-cycle fatigue of 2024 aluminum alloy

A.S. Yankin, A.V. Lykova, A.I. Mugatarov, V.E. Wildemann, A.V. Ilinykh
Center of Experimental Mechanics, Perm National Research Polytechnic University, Perm, Russian Federation
yas.cem@yandex.ru, https://orcid.org/0000-0002-0895-4912
cem.lykova@gmail.com, https://orcid.org/0000-0003-4873-6351
cem_mugatarov@mail.ru, https://orcid.org/0000-0002-2229-8181
wildemann@pstu.ru, https://orcid.org/0000-0002-6240-4022
ilinih@yandex.ru, https://orcid.org/0000-0001-9162-1053

ABSTRACT. In this paper, a previously developed modification of the Sines model of multiaxial fatigue is reduced to an invariant form. Model constants were determined for different sets of setup experiments. It was supposed to introduce an additional summand to account for the phase shift between loading modes. The model is used to describe the fatigue behavior of the 2024 aluminum alloy. Low-cycle fatigue tests under biaxial loading conditions are presented, with one mode changing cyclically and the other mode remaining constant in magnitude throughout the test. The results of cyclic durability prediction by the modified model provide good convergence.

KEYWORDS. Low-cycle fatigue; Experimental research; Complex stress state; Aluminum alloy; Fatigue life; Modified Sines model.

OPEN ACCESS

Citation: Yankin, A.S., Lykova, A.V., Mugatarov, A.I., Wildemann, V.E., Ilinykh, A.V., Influence of additional static stresses on biaxial low-cycle fatigue of 2024 aluminum alloy, Frattura ed Integrità Strutturale, 62 (2022) 180-193.

Received: 21.06.2022
Accepted: 24.08.2022
Online first: 25.08.2022
Published: 25.08.2022

INTRODUCTION

Nowadays, aluminum alloys are widely used due to their exceptional properties such as excellent plasticity, electrical and thermal conductivities. A wide diversity of applications can be found in aviation, machinery manufacturing, and other industries [1-2]. Some engineering components of construction elements are subjected to complex cyclic loads during operation, which might be a reason for the failure due to multiaxial fatigue [3]. Also, some notches, nicks, and dents can arise in products or parts during their exploitation which is related to, for example, foreign object damage [4-6]. Moreover, holes, fillets, grooves, and other geometrical features can be a part of structures. Such geometries can be the cause of inherent multiaxiality. In this respect, the stress or strain fields in the vicinity of stress or strain raiser are multiaxial even under uniaxial loads [7]. Thus, is crucial to consider the behavior of materials under the multiaxial loads in order to deliver fatigue life predictions.

The need in studying complex fatigue processes brought a number of experimental works, which used specialized equipment, specimens, and methods of multiaxial loading. The main load conditions referred to in the literature are biaxial tension of cross-shaped specimens [8], tension with torsion, bending with torsion of cylindrical specimens [9-12], as well as

three-axial tension with torsion and internal pressure of hollow specimens [9]. Apart from standard hourglass and tubular specimens, one tests weld joint specimens [13, 14, 18-21], specimens with notches, and other stress raisers [15-17].
Load factors can significantly affect the fatigue behavior of materials under the multiaxial influence, for instance, the change in the ratio of stress amplitudes [22-25], the phase angle between the modes of influence [22-26], the ratio of loading frequencies [22, 27, 28], average stresses in the cycle [29-37] and others. It should be noted that different dependencies of fatigue behavior on loading factors may be observed for various materials. In particular, an increase in the average stress leads to a decrease in fatigue strength. Such effect is pretty strong for brittle materials (e.g. cast iron) both in axial and in torsion [38]. However, it is lower in torsion than in axial for ductile materials such as steels and aluminum alloys [39].
Today, there are plenty of multiaxial models that can be used to predict the fatigue life/strength of various materials. These approaches can be classified as stress, strain, and strain energy density models. Some excellent reviews of multiaxial criteria are presented in works [40-42]. Also, the article of Papuga et al. should be noted [43]. It discusses the procedure in which the stress path is analyzed to provide relevant measures of parameters required by multiaxial criteria. The selection of this procedure affects the prediction results for out-of-phase cases. All these approaches are more or less accurate for different materials at various load paths, so it is important to validate multiaxial fatigue models in particular cases. In addition, it is vital to check the model application in case of notched and cracked bodies when stress concentrations exist.
In previous work, the authors proposed a modification of the Sines model to describe the fatigue behavior of 2024 aluminum alloy [22, 34]. However, this model is not invariant for the coordinate transformation in the case of disproportional loads, such as out-of-phase loads. In this paper, an approach to determine the model parameters to eliminate this drawback is proposed. Then, the model was validated using biaxial experimental data of 2024 aluminum alloy.

MULTIAXIAL FATIGUE MODEL

The previous model presented in [22, 34] has the issue that it is not invariant for the rotation of the coordinate system. In this regard, it is proposed to modernize the model in the following way.
In the general case, the stress tensor is some function of time:

$$\sigma_{ij} = \sigma_{ij}(t), t \geq 0 \tag{1}$$

In the case of periodic loads:

$$\sigma_{ij} = \sigma_{ij}(t), 0 \leq t \leq T; \sigma_{ij}(t) = \sigma_{ij}(t + nT), n \in N \tag{2}$$

where T is the loading period. Let us divide the tensor into constant and periodic components. Let each component of the stress tensor be known in some coordinate system. Enter the value:

$$\sigma_{ij}^{mean} = \frac{1}{T}\int_0^T \sigma_{ij}(t)\,dt \tag{3}$$

let us call it the average (constant) component of the stress tensor. In the case of rotation of the coordinate system:

$$\sigma_{kl}(t) = \alpha_{ki}\alpha_{lj}\sigma_{ij}(t)$$

$$\sigma_{kl}^{mean} = \frac{1}{T}\int_0^T \sigma_{kl}(t)\,dt = \frac{1}{T}\int_0^T \alpha_{ki}\alpha_{lj}\sigma_{ij}(t)\,dt = \alpha_{ki}\alpha_{lj}\frac{1}{T}\int_0^T \sigma_{ij}(t)\,dt = \alpha_{ki}\alpha_{lj}\sigma_{ij}^{mean} \tag{4}$$

which proves the tensor nature of the introduced value. Then the tensor of the periodically changing component of the stress tensor can be obtained:

$$\sigma_{ij}^{per}(t) = \sigma_{ij}(t) - \sigma_{ij}^{mean} \tag{5}$$

As a result, we obtain the decomposition of the stress tensor in the following form:

$$\sigma_{ij}(t) = \sigma_{ij}^{mean} + \sigma_{ij}^{per}(t) \tag{6}$$

It is worth noting that in the general case there may not exist a time moment t_{mean}, such that $\sigma_{ij}(t_{mean}) = \sigma_{ij}^{mean}$.
At each moment, the stress tensor is characterized by several quantities that do not depend on the choice of coordinate system. We choose the first invariant of the stress tensor I_1 and the second invariant of the stress deviator I_2 to use. Thus, these values, taking into account Eqn. (6), can be represented in the form:

$$I_1^{mean} = \sigma_{11}^{mean} + \sigma_{22}^{mean} + \sigma_{33}^{mean}$$

$$I_1^{per}(t) = \sigma_{11}^{per}(t) + \sigma_{22}^{per}(t) + \sigma_{33}^{per}(t)$$

$$I_2^{mean} = \frac{1}{6}\left(\left(\sigma_{11}^{mean} - \sigma_{22}^{mean}\right)^2 + \left(\sigma_{22}^{mean} - \sigma_{33}^{mean}\right)^2 + \left(\sigma_{11}^{mean} - \sigma_{33}^{mean}\right)^2 + 6\left(\left(\tau_{12}^{mean}\right)^2 + \left(\tau_{13}^{mean}\right)^2 + \left(\tau_{23}^{mean}\right)^2\right)\right) \tag{7}$$

$$I_2^{per}(t) = \frac{1}{6}\left(\left(\sigma_{11}^{per}(t) - \sigma_{22}^{per}(t)\right)^2 + \left(\sigma_{22}^{per}(t) - \sigma_{33}^{per}(t)\right)^2 + \left(\sigma_{11}^{per}(t) - \sigma_{33}^{per}(t)\right)^2\right) +$$
$$+\left(\tau_{12}^{per}(t)\right)^2 + \left(\tau_{13}^{per}(t)\right)^2 + \left(\tau_{23}^{per}(t)\right)^2$$

The first and third of these parameters are time-independent, the second and fourth depend on time. Let us determine the maximum and minimum values of the values to avoid the time dependence:

$$I_1^{max} = \max\left(I_1^{per}(t)\right)$$

$$I_1^{min} = \min\left(I_1^{per}(t)\right)$$

$$I_2^{max} = \max\left(I_2^{per}(t)\right) \tag{8}$$

$$I_2^{min} = \min\left(I_2^{per}(t)\right)$$

Taking into account expressions (7), (8), let us rewrite the model of multiaxial fatigue in the form:

$$A_1\frac{I_1^{max} - I_1^{min}}{2} + A_2 I_1^{mean} + \sqrt{A_3\frac{I_2^{max} + I_2^{min}}{2} + A_4 I_2^{mean}} \le 1 \tag{9}$$

DEFINING MODEL PARAMETERS

Let us define the model parameters (9). In the general case (with no additional assumptions), two fatigue curves obtained for symmetrical tension-compression and symmetrical cyclic torsion, a static tensile test, and a static torsion test are needed to calculate the parameters. Under static torsion:

$$I_2^{max} = I_2^{min} = I_1^{max} = I_1^{min} = I_1^{mean} = 0$$

$$I_2^{mean} = \tau^2 \tag{10}$$

$$A_4 I_2^{mean} \le 1 \rightarrow A_4 = \frac{1}{\tau_B^2}$$

Under static tension:

$$I_2^{max} = I_2^{min} = I_1^{max} = I_1^{min} = 0$$

$$I_1^{mean} = \sigma; I_2^{mean} = \frac{1}{3}\sigma^2 \tag{11}$$

$$\frac{1}{\sqrt{3}\tau_B}\sigma + A_2\sigma \le 1 \rightarrow A_2 = \frac{1}{\sigma_B} - \frac{1}{\sqrt{3}\tau_B}$$

where τ_b is the ultimate shear strength.
Under uniaxial cyclic symmetric torsion:

$$I_2^{min} = I_2^{mean} = I_1^{max} = I_1^{min} = I_1^{mean} = 0$$

$$I_2^{max} = \tau_a^2 \tag{12}$$

$$A_3 \frac{\tau_a^2}{2} \le 1 \rightarrow A_3 = \frac{2}{\left(\tau_f^{'}(2N)^{b_0}\right)^2}$$

where τ'_f, b_0 are material parameters determined from the fatigue curve for symmetrical cyclic torsion. Under uniaxial cyclic symmetric tension-compression:

$$I_2^{min} = I_2^{mean} = I_1^{mean} = 0$$

$$-I_1^{min} = I_1^{max} = \sigma_a; I_2^{max} = \frac{1}{3}\sigma_a^2 \tag{13}$$

$$\frac{\sigma_a}{\sqrt{3}\tau_f^{'}(2N)^{b_0}} + A_1\sigma_a \le 1 \rightarrow A_1 = \frac{1}{\sigma_f^{'}(2N)^{b_1}} - \frac{1}{\sqrt{3}\tau_f^{'}(2N)^{b_0}}$$

where σ'_f, b_1 are material parameters determined from the fatigue curve at symmetrical cyclic tension-compression. As a result, the model looks like this:

$$\sqrt{\frac{I_2^{max} + I_2^{min}}{\left(\tau_f^{'}(2N)^{b_0}\right)^2} + \frac{I_2^{mean}}{\tau_B^2}} + \left(\frac{1}{\sigma_f^{'}(2N)^{b_1}} - \frac{1}{\sqrt{3}\tau_f^{'}(2N)^{b_0}}\right)\frac{I_1^{max} - I_1^{min}}{2} + \left(\frac{1}{\sigma_B} - \frac{1}{\sqrt{3}\tau_B}\right)I_1^{mean} \le 1 \tag{14}$$

If there is one fatigue curve and a point on another curve, we can assume that they are equidistant, then $b_1=b_0$, the model will be rewritten in the form:

$$\sqrt{\frac{I_2^{max}+I_2^{min}}{\left(\tau_f^{'}(2N)^{b_0}\right)^2}+\frac{I_2^{mean}}{\tau_B^2}}+\left(\frac{\tau_f^{'}}{\sigma_f^{'}}-\frac{1}{\sqrt{3}}\right)\frac{1}{\tau_f^{'}(2N)^{b_0}}\frac{I_1^{max}-I_1^{min}}{2}+\left(\frac{1}{\sigma_B}-\frac{1}{\sqrt{3}\tau_B}\right)I_1^{mean}\le 1 \tag{15}$$

If there is one fatigue curve, we can assume that the tensile-compression and torsional curves coincide, then $\sigma'_f=\sqrt{3}\tau'_f$, the model will have the form:

$$\sqrt{\frac{I_2^{max}+I_2^{min}}{\left(\tau_f^{'}(2N)^{b_0}\right)^2}+\frac{I_2^{mean}}{\tau_B^2}}+\left(\frac{1}{\sigma_B}-\frac{1}{\sqrt{3}\tau_B}\right)I_1^{mean}\le 1 \tag{16}$$

If there is only one static test, we can take $\sigma_B=\sqrt{3}\tau_B$, the model will look like this:

$$\frac{I_2^{max}+I_2^{min}}{\left(\tau_f^{'}(2N)^{b_0}\right)^2}+\frac{I_2^{mean}}{\tau_B^2}\le 1 \tag{17}$$

CONSIDERATION OF THE PHASE ANGLE BETWEEN LOADING MODES

It can be shown that in the variants of notation (14)-(17) the model of multiaxial fatigue will not consider the phase shift between the normal and tangential stress components, which does not always correspond to the experimental data. In this regard, let us introduce an additional summand into the radical expression:

$$A_1\frac{I_1^{max}-I_1^{min}}{2}+A_2I_1^{mean}+\sqrt{A_3\frac{I_2^{max}+I_2^{min}}{2}+A_4I_2^{mean}+A_5I_2^{min}}\le 1 \tag{18}$$

The last term of the radical expression will be nonzero only if there is a phase shift between the tangential and normal loading modes. The setup experiment to determine the constant A_5 can be as follows:

$$\begin{gathered}\sigma_{11}=\sigma_a\sin(\omega t);\tau_{12}=\tau_a\sin\left(\omega t+\frac{\pi}{2}\right)\\ \sigma_{22}=\sigma_{33}=\tau_{13}=\tau_{23}=0;\sigma_a=\sqrt{3}\tau_a\end{gathered} \tag{19}$$

thus

$$\begin{gathered}I_1^{max}-I_1^{min}=2\sigma_a;I_1^{mean}=0;I_2^{mean}=0\\ I_2^{per}(t)=\frac{1}{3}\left(\sigma_a\sin(\omega t)\right)^2+\left(\tau_a\sin\left(\omega t+\frac{\pi}{2}\right)\right)^2=\tau_a^2\left(\left(\sin(\omega t)\right)^2+\left(\cos(\omega t)\right)^2\right)=\tau_a^2\\ I_2^{max}=I_2^{min}=\tau_a^2\\ A_1\sqrt{3}\tau_a+\sqrt{A_3\tau_a^2+A_5\tau_a^2}\le 1\rightarrow A_5=\left(\frac{1}{\tau_{phase}^{'}(2N)^{b_{phase}}}-\frac{\sqrt{3}}{\sigma_f^{'}(2N)^{b_1}}+\frac{1}{\tau_f^{'}(2N)^{b_0}}\right)^2-\frac{2}{\left(\tau_f^{'}(2N)^{b_0}\right)^2}\end{gathered} \tag{20}$$

where τ'_{phase}, b_{phase} are material parameters determined from the fatigue curve for the described experiment (19). If the material is not sensitive to phase shift, we can assume $A_5 = 0$.
The fatigue failure criteria based on stresses are not able to take into account the effect of cyclic hardening or softening. If the fatigue tests are carried out under stress controlled system, the effect of cyclic hardening or softening is visible only in strain history, which is not taken into account in the fatigue failure criteria based on stresses.

MODEL VALIDATION

The model validation was carried out using experimental data [26, 29, 44-49]. For each data set mean absolute error was calculated taking into account and excluding the phase shift effect (MAE_{phase} and $MAE_{no\ phase}$). Determining model parameters are shown in Tab. 1. A comparison between predicted fatigue lives with taking into account and excluding the phase shift effect is shown in Fig. 1. It can be concluded that consideration of the phase shift allows improving the accuracy of the fatigue life prediction.

Data set	1	2	3	4
Authors	A. Fatemi et al [29, 44]	Y.-Y. Wang et al [26]	T.-X. Xia et al [45-48]	X.-W. Wang et al [49]
τ'_f, *MPa*	460.0	600.8	642.3	
b_0	-0.082	-0.104	-0.118	
σ'_f, *MPa*	1199.3	951.9	1324.8	
b_1	-0.133	-0.102	-0.145	
τ_B, *MPa*	283.0	290.0	283.0	
σ_B, *MPa*	450.0	545.0	450.0	
τ'_{phase}, *MPa*	595.8	583.8	690.3	
b_{phase}	-0.140	-0.142	-0.171	
$MAE_{no\ phase}$	0.240	0.210	0.117	0.162
MAE_{phase}	0.218	0.150	0.110	0.157

Table 1: Calculated model parameters.

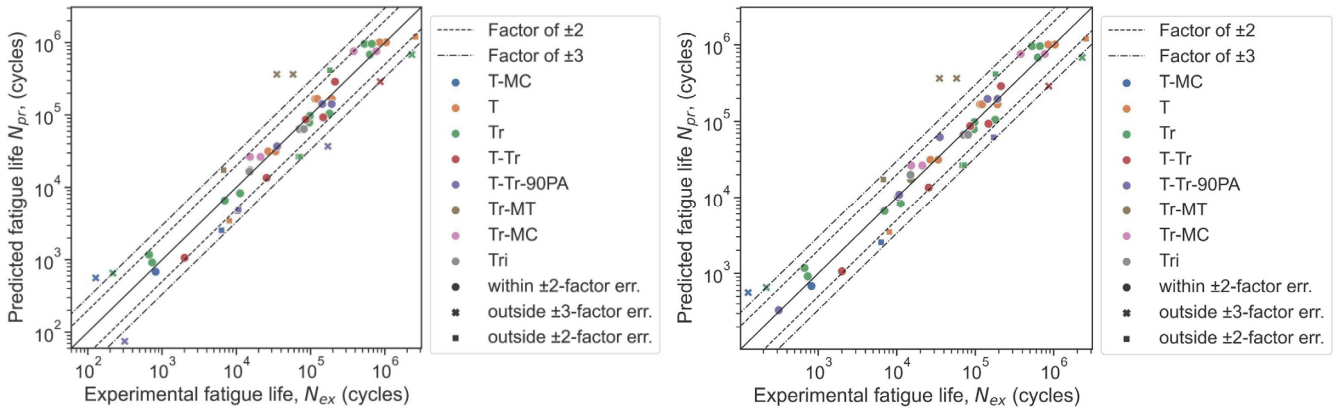

a b

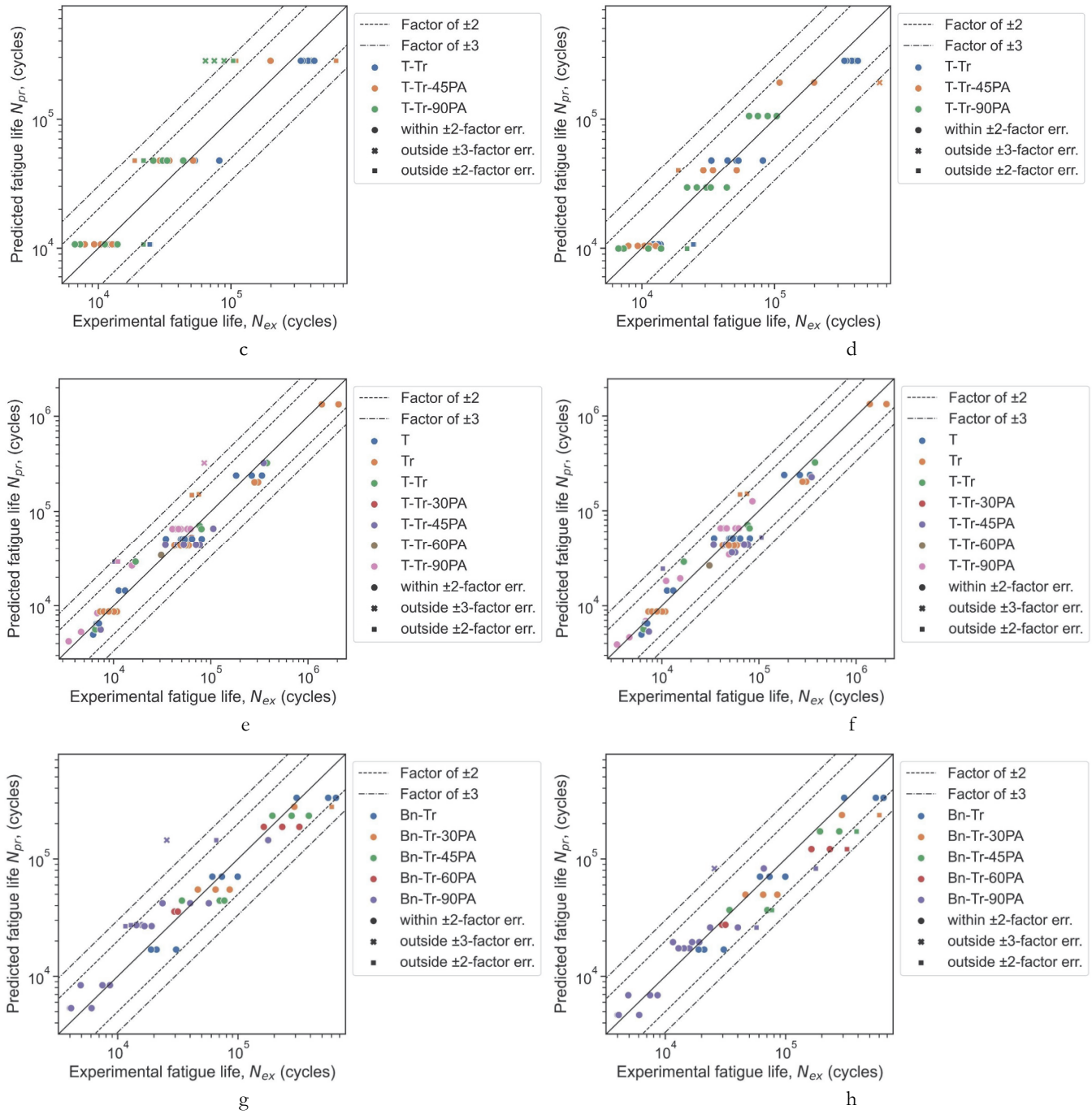

Figure 1: Comparison of experimental and predicted fatigue live with taking into account (b, d, f, h) and excluding the phase shift effect (a, c, e, g) for data sets: 1 (a, b), 2 (c, d), 3 (e, f) and 4 (g, h).

EXPERIMENTAL PROCEDURE AND RESULTS

Of particular interest is the study of low-cycle fatigue in the presence of the second component of small magnitude, which can occur under difficult operating conditions. Experiments on low-cycle fatigue under biaxial strain conditions, with one of the modes (normal or tangential stress) changing cyclically and the other mode remaining constant in magnitude during the test, were performed at room temperature on an Instron 8850 servohydraulic system at the PNRPU Center of Experimental Mechanics. During fatigue testing on servohydraulic machines, the moving parts of the system experience

acceleration, so that in addition to the force applied to the sample, the load cell also records the force caused by the movement of the grips and fixtures installed. These test systems use sensors, particularly Dynacell sensors, which have an accelerometer mounted directly on the load axis to minimize errors due to inertial forces. The deformations were recorded using an Epsilon 3550-010M dual-axis extensometer with a 10-mm measurement base with a full range of ± 5.0 mm for axial displacement and ± 3° for shear angle. We performed pre-cycling in the elastic zone and determined Young's modulus and shear modulus under static loading to verify that the extensometer was correctly installed.
2024 aluminum alloy was used as the test material. The chemical composition of the alloy consists (in percent) of Fe, Si<0.5, Mn 0.3-0.9, Cr<0.1, Ti<0.15, Al 90.9-94.7, Cu 3.8-4.9, Mg 1.2-1.8, Zn<0.25, Ti+Zr<0.2, other elements<0.15. Fatigue tests were carried out on thin-walled samples with an annular cross-section in the working part. A sketch of the sample is shown in Fig. 2.

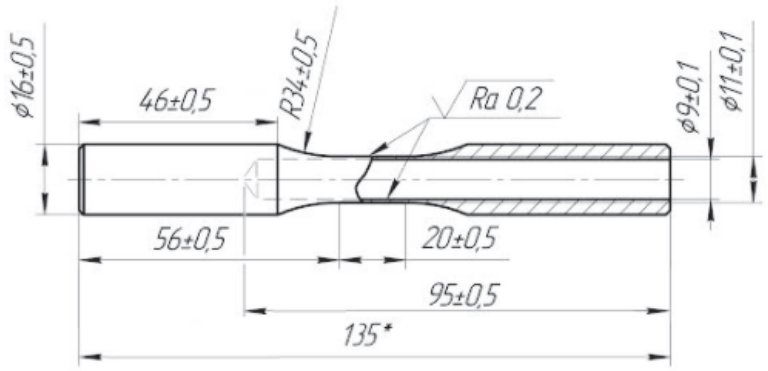

Figure 2: Specimen geometry (in mm).

Three different levels of constant stress components were selected for cyclic tests to assess their effect on the durability of aluminum alloy. The values of the constant components were chosen from the tensile and torsional strain diagrams of aluminum alloy samples. The specimens were tested at two levels of stress amplitude for each biaxial strain scheme. Tests were conducted at room temperature with a test frequency of 1 Hz. The specified cyclic loading parameters are presented in Tab. 2.

Constant normal stress σ_m, *MPa*	Constant shear stress τ_m, *MPa*	Normal stress amplitude σ_a, *MPa*	Shear stress amplitude τ_a, *MPa*	Stress range $\sigma_r(\tau_r)$, *MPa*	Tested samples number	Number of cycles to failure, *N*
0	70	275	0	550	4	3411, 3598, 3347, 5344
0	110	275	0	550	3	1834, 1804, 1824
0	160	275	0	550	1	1144
0	70	215	0	430	3	51277, 26912, 30470
0	110	215	0	430	2	18819,16668
100	0	0	150	300	2	9545, 4825
200	0	0	150	300	2	5450, 5170
350	0	0	150	300	2	1910, 2978
100	0	0	115	230	3	106493, 77745, 82800
200	0	0	115	230	2	24468, 49650
350	0	0	115	230	2	11234, 11283

Table 2: Summary fatigue tests.

Experimental studies of low-cycle fatigue under constant component conditions resulted in fatigue life values at different values of stress amplitudes. The results obtained, shown in Fig. 3 and 4, indicate a significant effect of constant components on one of the modes during biaxial low-cycle fatigue on cyclic durability.

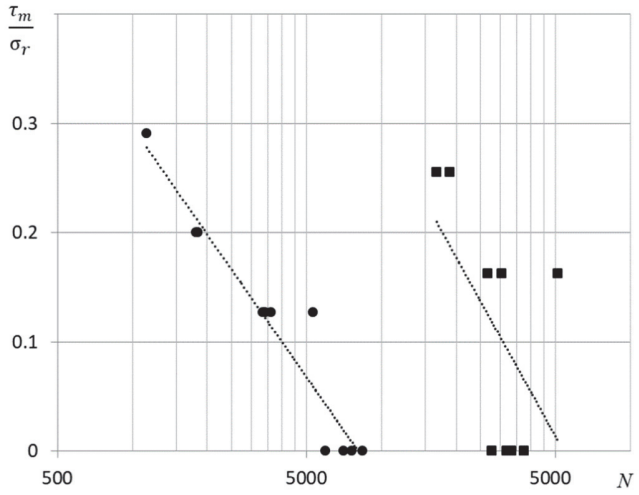

Figure 3: Dependence of fatigue life on the level of constant value tangential stresses related to the stress range at the amplitude of normal stresses: σ_a = 270 MPa (●), σ_a = 215 MPa (■).

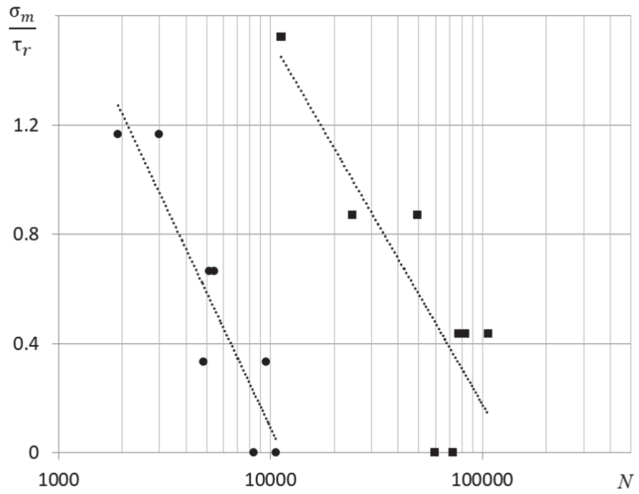

Figure 4: Dependence of fatigue life on the level of constant values normal stresses related to the stress range at the amplitude of tangential stress amplitudes at: τ_a=150 MPa (●),$_a$ =115 MPa (■).

It is shown that at certain ratios of constant and cyclic components, the durability decreases by an order of magnitude.

CALCULATION OF FATIGUE LIFE USING THE PROPOSED MODEL

The experimental data obtained are used to test the proposed model (9) with A_5 = 0. Static tensile tests, static torsion tests, symmetrical cyclic tension-compression, and symmetrical cyclic torsion tests were performed to find the constants included in this model.

The A_2 and A_4 model parameters include ultimate tensile and shear strength: the ultimate tensile strength σ_B of the alloy is equal to 450 MPa; the ultimate shear strength τ_B of the alloy is equal to 280 MPa. The coefficients included in the A_1 and

A_3 parameters were determined from the fatigue curves obtained in symmetrical tensile-compression (Fig. 5a) and symmetrical torsion (Fig. 5b).

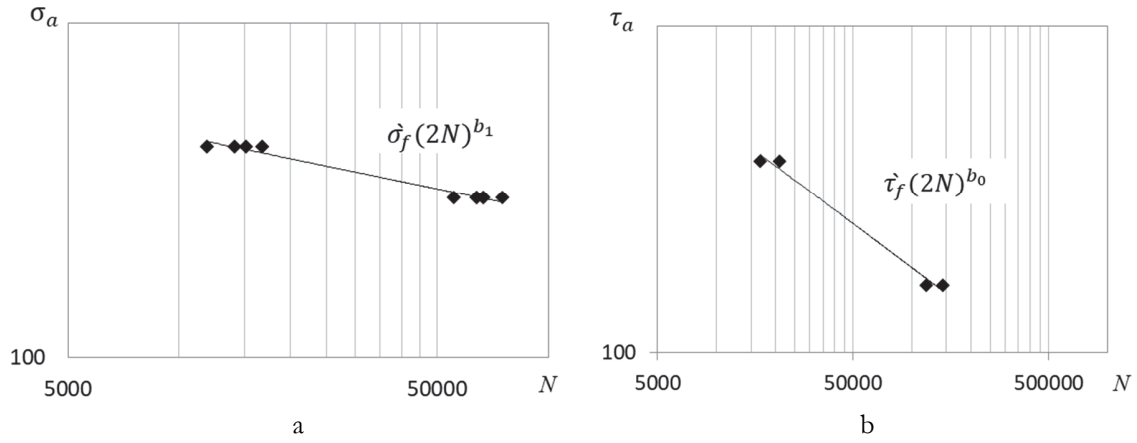

Figure 5: Fatigue curves.

Coefficients σ'_f = 1270 MPa, τ'_f = 566 MPa, and exponents b_1 = -0.160, b_0 = -0.135.
The results of fatigue life calculations using the proposed model are presented at Fig.6. The figure shows graphs of the dependence of the predicted durability on the experimental one. The colored dots indicate tests at different values of normal and tangential stress amplitudes. Dotted and dashed lines on the graphs show ±2 and ±3 factor errors.

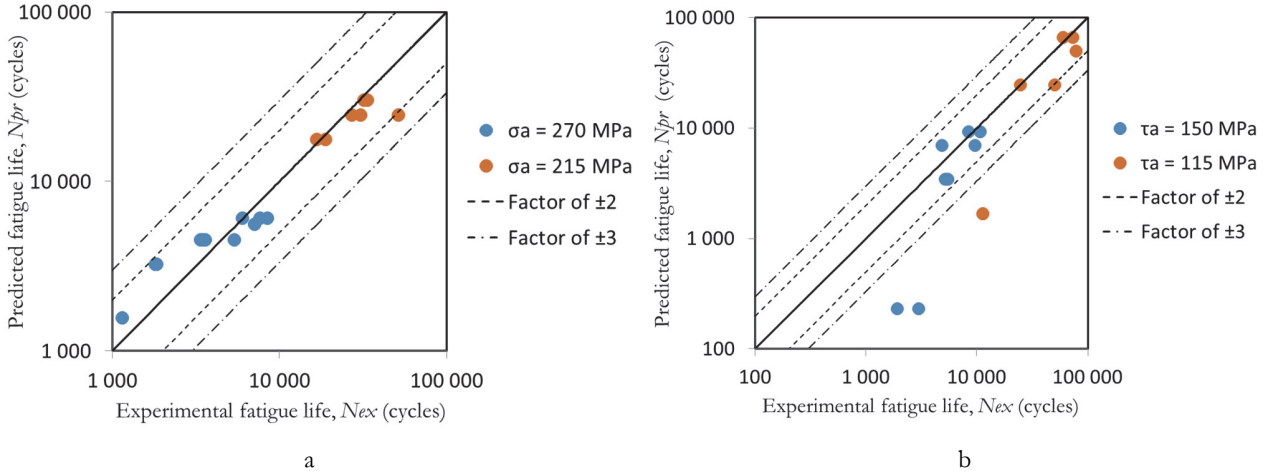

Figure 6: Results of cyclic durability prediction according to the proposed model for samples of 2024 aluminum alloy: cyclic torsion with various mean normal stress values (a); cyclic tension-compression with various mean shear stress values (b).

The above graphs show that when loaded with superimposed mean shear stress, all dots lie within the ±3 factor interval. This indicates that this model predicts well the fatigue life of the aluminum alloy under such influences. However, when loaded with superimposed mean normal stress, three points fall outside the ±3 factor interval. In this case, the values of constant normal stresses for these dropout points were 350 MPa, which is close to the yield strength of the material. As a result, we can conclude that the model predicts the result quite well at values of constant normal stresses less than the yield strength of the material and becomes significantly conservative at values of constant normal stresses close to and greater than the yield strength. In addition, it is worth noting the work of J. Papuga [50], in which the authors also point out similar problems with this model. Thus, it might be worth introducing an additional term responsible for the one-sided accumulation of deformations (ratcheting) into the model parameters to refine the prediction of the proposed model in the future. This term will probably allow a better description of the experimental data at high values of the static stress components.

CONCLUSIONS

The modernized Sines model proposed by the authors is reduced to an invariant form. The time-varying stress tensor is decomposed into constant and periodic components. The maximum and minimum values of the first and second invariants of these components were used to record the model. It was supposed to introduce an additional summand to account for the phase shift between loading modes. Model constants were determined for different sets of setup experiments. The proposed model was validated using number of data sets, which were taken from literature results. Fatigue tests on samples made of 2024 aluminum alloy were carried out. It is shown that the model describes well the fatigue behavior of the material under symmetrical tension-compression with superimposed mean shear stress and under symmetrical torsion with superimposed mean normal stress at values of constant normal stresses less than the yield stress. At values of constant normal stresses close to and greater than the yield strength, the model becomes substantially conservative.

ACKNOWLEDGEMENTS

The work was carried out in Perm National Research Polytechnic University with the financial support of the Russian Foundation for Basic Research (project number 19-38-90270) and within the State Assignment of the Ministry of Science and Higher Education of the Russian Federation (No. FSNM-2020-0027).

NOMENCLATURE

b_0	shear fatigue strength exponent
b_1	axial fatigue strength exponent
b_{phase}	90 out-of-plane fatigue strength exponent
I_1^{max}	maximum value of the first invariant of the stress tensor σ_{ij}^{per}
I_1^{mean}	first invariant of the stress tensor σ_{ij}^{mean}
I_1^{min}	minimum value of the first invariant of the stress tensor σ_{ij}^{per}
I_2^{max}	maximum value of the second invariant of the stress deviator σ_{ij}^{per}
I_2^{mean}	second invariant of the stress deviator σ_{ij}^{mean}
I_2^{min}	minimum value of the second invariant of the stress deviator σ_{ij}^{per}
$MAE_{no\ phase}$	mean absolute error excluding the phase shift effect
MAE_{phase}	mean absolute error taking into account the phase shift effect
N	number of cycles to failure
t	time
T	cycle period
a_{kl}	coordinate system rotation matrix
σ_a	normal stress amplitude
σ_B	tensile strength
σ_{ij}	stress tensor
σ_{ij}^{mean}	average component of the stress tensor
σ_{ij}^{per}	periodically changing component of the stress tensor
σ'_f	axial fatigue strength coefficient
σ_m	constant normal stress
σ_r	normal stress range
τ_a	shear stress amplitude
τ_B	torsional strength
τ'_f	shear fatigue strength coefficient
τ_m	constant shear stress
τ'_{phase}	90 out-of-plane fatigue strength coefficient
τ_r	shear stress range
ω	cyclic frequency

REFERENCES

[1] Liao, Y.S., Li, Y.B., Pan, Q., Huang, M.H. and Zhou, C. (2018). Residual fatigue life analysis and comparison of an aluminum lithium alloy structural repair for aviation applications, Eng. Fract. Mech., 194, pp. 262–280. DOI: 10.1016/j.engfracmech.2018.03.020.

[2] Fahim, J., Hadavi, S.M.M., Ghayour, H. and Hassanzadeh Tabrizi, S.A. (2019). Cavitation erosion behavior of super-hydrophobic coatings on Al5083 marine aluminum alloy, Wear, 424-425, pp. 122–132. DOI: 10.1016/j.wear.2019.02.017.

[3] Esmaeili, F., Chakherlou, T.N. and Zehsaz, M. (2014). Prediction of fatigue life in aircraft double lap bolted joints using several multiaxial fatigue criteria, Mater. Des., 59, pp. 430-438. DOI:10.1016/j.matdes.2014.03.019.

[4] Baragetti, S., Gerosa, R., Rivolta, B., Silva, G. and Tordini, F. (2011). Fatigue behavior of foreign object damaged 7075 heat treated aluminum alloy coated with PVD WC/C, Proc. Engineering, 10, pp. 3375-3380, DOI: 10.1016/j.proeng.2011.04.556.

[5] Ruschau, J., Thompson, S.R., and Nichola, T. (2003). High cycle fatigue limit stresses for airfoils subjected to foreign object damage, Int. J. Fatigue, 25(9–11), pp. 955-962. DOI:10.1016/S0142-1123(03)00135-X.

[6] Chen, X. (2005). Foreign object damage on the leading edge of a thin blade, Mech Mater, 37(4), pp. 447-457. DOI: 10.1016/j.mechmat.2004.03.005.

[7] Susmel, L. (2009). Multiaxial notch fatigue: from nominal to local stress-strain quantities, Woodhead Publishing.

[8] Shanyavskiy, A. (2011). Fatigue cracking simulation based on crack closure effects in Al-based sheet materials subjected to biaxial cyclic loads, Eng. Fract. Mech., 78(8), pp. 1516-1528. DOI:10.1016/j.engfracmech.2011.01.019.

[9] Malek, B., Mabru, C. and Chaussumier, M. (2020). Fatigue behavior of 2618-T851 aluminum alloy under uniaxial and multiaxial loadings, Int. J. Fatigue, 131, 105322. DOI:10.1016/j.ijfatigue.2019.105322.

[10] Itoh, T. and Yang, T. (2011). Material dependence of multiaxial low cycle fatigue lives under non-proportional loading, Int. J. Fatigue, 33(8), pp. 1025-1031. DOI: 10.1016/j.ijfatigue.2010.12.001.

[11] Itoh, T., Murashima, K. and Hirai, T. (2007). Material dependence of multiaxial low cycle fatigue properties under non-proportional loading, J. Soc. Mater. Sci. Jpn., 56 (2), pp. 157-163.

[12] Lomakin, E.V., Tretyakov, M.P., Ilinykh, A.V. and Lykova, A.V. (2019). Mechanical behavior of X15CrNi12-2 structural steel under biaxial low-cycle fatigue at normal and elevated temperatures, PNIPU Mech. Bulletin, 1, pp. 78-87. DOI: 10.15593/perm.mech/2019.1.07.

[13] Ribeiro, A.S. and De Jesus, A.M.P. (2011). Fatigue Behaviour of Welded Joints Made of 6061-T651 Aluminium Alloy, Aluminium Alloys, Theory and Applications, IntechOpen, London. DOI: 10.5772/14489.

[14] Li, H., Gao, J. and Li, Q. (2018). Fatigue of Friction Stir Welded Aluminum Alloy, Appl. Sci., 8(12), 2626. DOI: 10.3390/app8122626.

[15] Zhao, B., Xie, L., Wang, L., Hu, Z., Zhou, S. and Bai, X. (2018) A new multiaxial fatigue life prediction model for aircraft aluminum alloy, Int. J. Fatigue, 143, 105993. DOI: 10.1016/j.ijfatigue.2020.105993.

[16] Htoo, T., Miyashita, A., Y., Otsuka, Y., Mutoh, Y. and Sakurai, S. (2016). Variation of local stress ratio and its effect on notch fatigue behavior of 2024-T4 aluminum alloy, Int. J. Fatigue, 88, pp. 19-28. DOI:10.1016/j.ijfatigue.2016.03.001.

[17] Gillham, B., Yankin, A., McNamara, F., Tomonto, C., Taylor, D. and Lupoi R. (2021). Application of the Theory of Critical Distances to predict the effect of induced and process inherent defects for SLM Ti-6Al-4V in High Cycle Fatigue, CIRP Ann. Manuf. Technol., 70(1), pp. 171–174. DOI: 10.1016/j.cirp.2021.03.004.

[18] Han, Q., Wang, P. and Lu. Y. (2019). Low-cycle multiaxial fatigue behavior and life prediction of Q235B steel welded material, Int. J. Fatigue, 127, pp. 417-430. DOI: 10.1016/j.ijfatigue.2019.06.027.

[19] Rodriguez, R.I., Jordon, J.B., Allison, P.G., Rushing, T. and Garcia, L. (2016). Low-cycle fatigue of dissimilar friction stir welded aluminum alloys, Mater. Sci. Eng. A, 654, pp. 236-248. DOI: 10.1016/j.msea.2015.11.075.

[20] Yousefi, F., Witt, M. and Zenner, H. Fatigue strength of welded joints under multiaxial loading: experiments and calculations, Fatigue Fract. Eng. Mater. Struct., 24(5), pp. 339-355. DOI: 10.1046/j.1460-2695.2001.00397.x.

[21] Pei, X., Ravi, S.K., Dong, P., Li, X. and Zhou, X. (2022). A multi-axial vibration fatigue evaluation procedure for welded structures in frequency domain, Mech. Syst. Signal Process., 167, 108516. DOI: 10.1016/j.ymssp.2021.108516.

[22] Yankin, A.S., Wildemann, V.E. and Mugatarov, A.I. (2021). A.I. Influence of different loading paths on the multiaxial fatigue behavior of 2024 aluminum alloy under the same amplitude values of the second invariant of the stress deviator tensor, Frat. ed Integrita Strutt., 55, pp. 327-335. DOI: 10.3221/IGF-ESIS.55.25.

[23] Zhang, J., Shi, X. and Fei, B. (2012). High cycle fatigue and fracture mode analysis of 2A12-T4 aluminum alloy under out of-phase axial-torsion constant amplitude loading, Int. J. Fatigue, 38, pp. 144-154. DOI: 10.1016/j.ijfatigue.2011.12.017.
[24] Wang, Q., Xin, C., Sun, Q., Xiao, L. and Sun, J. (2018). Biaxial fatigue behavior of gradient structural purity titanium under in-phase and out-of-phase loading, Int. J. Fatigue, 116, pp. 602-609. DOI: 10.1016/j.ijfatigue.2018.07.015.
[25] Liu, T., Shi, X., Zhang, J. and Fei, B. (2019). Crack initiation and propagation of 30CrMnSiA steel under uniaxial and multiaxial cyclic loading, Int. J. Fatigue, 122, pp. 240-255. DOI: 10.1016/j.ijfatigue.2019.02.001
[26] Wang, Y.-Y. and Yao, W.-X. (2006). A multiaxial fatigue criterion for various metallic materials under proportional and nonproportional loading, Int. J. Fatigue, 28(4), pp. 401-408. DOI: 10.1016/j.ijfatigue.2005.07.007
[27] Skibicki, D. and Pejkowski, L. (2017). Low-cycle multiaxial fatigue behaviour and fatigue life prediction for CuZn37 brass using the stress-strain models, Int. J. Fatigue, 102, pp. 18-36. DOI: 10.1016/j.ijfatigue.2017.04.011.
[28] Pejkowski, L., Skibicki, D. and Seyda, J. (2018). Stress-strain response and fatigue life of a material subjected to asynchronous loadings, AIP Conference Proceeding, 2028, 020016. DOI: 10.1063/1.5066406.
[29] Gates, N.R. and Fatemi, A. (2017). On the consideration of normal and shear stress interaction in multiaxial fatigue damage analysis, Int. J. Fatigue, 100, pp. 322-336. DOI: 10.1016/j.ijfatigue.2017.03.042.
[30] Wildemann, V.E., Tretyakov, M.P., Staroverov, O.A. and Yankin, A.S. (2018). Influence of the biaxial loading regimes on fatigue life of 2024 aluminum alloy and 40CrMnMo steel, PNRPU Mech. Bull., 4, pp. 169-177. DOI: 10.15593/perm.mech/2018.4.16.
[31] Sines, G. (1955). Failure of materials under combined repeated stresses with superimposed static stress, Washington, National Advisory Committee for Aeronautics (N.A.C.A), 6.
[32] Mocilnik, V., Gubeljak, N. and Predan, J. (2017). The Influence of a Static Constant Normal Stress Level on the Fatigue Resistance of High Strength Spring Steel, Theor. Appl. Fract. Mech., 91, pp. 139-147. DOI: 10.1016/j.tafmec.2017.06.002.
[33] Papuga, J. and Halama, R. (2018). Mean stress effect in multiaxial fatigue limit criteria. Arch. Appl. Mech., pp. 1-12. DOI: 10.1007/s00419-018-1421-7.
[34] Yankin, A., Wildemann, V., Belonogov and Staroverov, O. (2020). Influence of static mean stresses on the fatigue behavior of 2024 aluminum alloy under multiaxial loading, Frat. ed Integrita Strutt, 14(51), pp. 151-163. DOI: 10.3221/IGF-ESIS.51.12.
[35] Zhu, H., Wu, H., Lu, Y. and Zhong, Z. (2019). A novel energy-based equivalent damage parameter for multiaxial fatigue life prediction, Int. J. Fatigue, 121, pp. 1-8. DOI: 10.1016/j.ijfatigue.2018.11.025.
[36] Carrion, P.E., Shamsaei, N., Daniewicz, S.R. and Moser, R.D. (2017). Fatigue behavior of, Ti-6Al-4V ELI including mean stress effects, Int. J. Fatigue, 99(1), pp. 87-100. DOI:10.1016/j.ijfatigue.2017.02.013.
[37] Kluger, K. (2015). Fatigue life estimation for 2017A-T4 and 6082-T6 aluminum alloys subjected to bending-torsion with mean stress, Int. J. Fatigue, 80, pp. 22-29. DOI:10.1016/j.ijfatigue.2015.05.005.
[38] Tovo, R., Lazzarin, P., Berto, F., Cova, M. and Maggiolini, E. (2014). Experimental investigation of the multiaxial fatigue strength of ductile cast iron, Theor. Appl. Fract. Mech., 73, pp. 60-67. DOI: 10.1016/j.tafmec.2014.07.003.
[39] Pallarés-Santasmartas, L., Albizuri, J., Avilés, A., Saintier, N. and Merzeau, J. (2018). Influence of mean shear stress on the torsional fatigue behaviour of 34CrNiMo6 steel, Int. J. Fatigue, 113, pp. 54-68. DOI: 10.1016/j.ijfatigue.2018.04.008.
[40] Karolczuk, A. and Macha, E. (2005). A Review of Critical Plane Orientations in Multiaxial Fatigue Failure Criteria of Metallic Materials. Int J Fract, 134(267). DOI: 10.1007/s10704-005-1088-2.
[41] Milella, P. P. (2013). Fatigue and Corrosion in Metals, Springer Milan Heidelberg New York Dordrecht London. DOI: 10.1007/978-88-470-2336-9
[42] Carpinteri, A., Spagnoli, A., and Vantadori, S. (2017). A review of multiaxial fatigue criteria for random variable amplitude loads, Fatigue Fract. Engng Mater. Struct, 40(7), pp. 1007-1036. DOI: 10.1111/ffe.12619.
[43] Papuga, J., Cízová, E. and Karolczuk, A. (2021). Validating the Methods to Process the Stress Path in Multiaxial High-Cycle Fatigue Criteria. Materials 14(1), 206. DOI: 10.3390/ma14010206.
[44] Sharifimehr, S. and Fatemi, A. (2019). Interaction Between Normal and Shear Stresses and Its Effect on Multiaxial Fatigue Behavior. MATEC Web of Conferences, 300, 16007. DOI: 10.1051/matecconf/201930016007.
[45] Xia, T. and Yao, W. (2013). Comparative research on the accumulative damage rules under multiaxial block loading spectrum for 2024-T4 aluminum alloy. Int. J. Fatigue, 48, pp. 257–265. DOI: 10.1016/j.ijfatigue.2012.11.004.
[46] Xia, T., Yao, W., Ji, Y. F. and Wang, C. J. (2015). Study on the accumulative fatigue damage rules under multiaxial two-stage step spectra constructed by loadings with similar lives. Fatigue Fract. Eng. Mater. Struct, 38(7), pp. 838–850. DOI: 10.1111/ffe.12256.

[47] Xia, T., Yao, W. and Lu, J-G. (2014). On the Shear Stress Parameter of Thin-walled Tubular Specimens under Torsional Loading. Procedia Engineering, 74, pp. 191–198. DOI: 10.1016/j.proeng.2014.06.249.

[48] Xia, T., Yao, W., Zou, J., and Gao, D. (2015). A novel accumulative fatigue damage model for multiaxial step spectrum considering the variations of loading amplitude and loading path. Fatigue Fract. Eng. Mater. Struct, 39(2), pp. 194–205. DOI: 10.1111/ffe.12349.

[49] Wang, X-W. and Shang, De-G. (2016). Determination of the critical plane by a weight-function method based on the maximum shear stress plane under multiaxial high-cycle loading. Int. J. Fatigue, 90, pp. 36-46. DOI: 10.1016/j.ijfatigue.2016.04.010.

[50] Papuga, J., Nesládek, M., Hasse, A., Cízová, E. and Suchý, L. (2022). Benchmarking Newer Multiaxial Fatigue Strength Criteria on Data Sets of Various Sizes. Metals, 12(2), 289. DOI: 10.3390/met12020289.